Process $\pi p \to \pi \pi N$ at high energies and moderate momenta transferred to the nucleon and the determination of parameters of the $f_0(980)$ and $f_0(1300)$

V.V. Anisovich and A.V. Sarantsev (November 16, 2018)

We present the results of simultaneous analysis of the S-wave $\pi\pi$ -spectra in the reactions $\pi^-p \to (\pi\pi)_S$ n at $p_{lab}=38$ GeV/c (GAMS) and $\pi^-p \to (\pi\pi)_S$ n at $p_{lab}=18$ GeV/c (E852 Collaboration) at moderate momenta transferred to the nucleon, $|t| \lesssim 1.5$ (GeV/c)². The t-distributions are described by the reggeized π - and a_1 -exchanges provided by the leading and daughter trajectories, while the $M_{\pi\pi}$ -spectra are determined by a set of scalar-isoscalar resonances. With $M_{\pi\pi}$ -distributions averaged over t-intervals, we have found several solutions given by different t-channel exchange mechanisms at $|t| \sim (0.5-1.5)$ (GeV/c)², with resonance parameters close to each other. We conclude that despite a poor knowledge of the structure of the t-exchange, the characteristics of resonances such as masses and widths can be reliably determined using the processes under discussion. As to pole positions, we have found $(1031 \pm 10) - i(35 \pm 6)$ MeV for $f_0(980)$ and $(1315 \pm 20) - i(150 \pm 30)$ MeV for $f_0(1300)$.

I. INTRODUCTION

The reactions of meson production in meson–nucleon collisions such as $\pi p \to \pi \pi N$, $K\bar{K}N$, $\eta \eta N$ and $KN \to \pi KN$ are traditionally a source of information about resonances in the two-meson spectra, namely, $\pi \pi$, $K\bar{K}$, $\eta \eta$, πK , see e.g. [1–3]. So it would be important to know what resonance characteristics could be reliably determined from these reactions and where one may encounter problems.

A set of the K-matrix analyses [4–10] are based on the three-meson production data in the $p\bar{p}$ annihilation, together with data on the two-meson production in meson-nucleon high energy collisions. The GAMS data for the reaction $\pi^-p \to \pi^0\pi^0 n$ at $p_{lab} = 38 \text{ GeV/c}$ [3], which represent the production of $\pi^0\pi^0$ at relatively large momentum transfers, are important for the investigation of 1200–1400 MeV mass region: at $|t| \sim 0.5 - 1.0 \text{ (GeV/c)}^2$ a distinct peak was seen near 1300 MeV in $\pi^0\pi^0$ spectra.

The resonance $f_0(1300)$ (denoted as $f_0(1370)$ in the compilation [11]) had been observed in the analysis of the $\pi\pi$ and $\eta\eta$ spectra obtained from the annihilation of $p\bar{p}(at\,rest,liquid\,H_2)\to\pi^0\pi^0\pi^0$, $\pi^0\pi^0\eta$, $\pi^0\eta\eta$ [12–14]. In the most comprehensive analysis [13], where both resonance production (pole singularities of the amplitude) and the meson rescattering in the final state (logarithmic singularities of the amplitude [15]) were taken into account, the magnitude for the complex-valued mass was found to be $M-i\Gamma/2=(1335\pm40)-i(127^{+30}_{-20})$ MeV . In the analyses presented in [12,14], a simplified fitting procedure was carried out, without accounting for logarithmic singularities: one obtained $(1340\pm40)-i(127^{+30}_{-20})$ MeV [14]. In the Crystal Barrel Collaboration paper [12] the claimed mass was 1365^{+20}_{-55} MeV reflecting an attempt to make it closer to a scalar resonance which was then defined at 1430-i125 MeV [16]. Before that, the existence of a scalar-isoscalar resonance was also claimed to be at 1430-i73 MeV [17] or 1420-i110 MeV [18].

But now it became obvious that the mass shift towards higher value is due to not sufficiently correct account for the interference "resonance/background": the fact that, just due to a considerable interference in the $\pi\pi$ S-wave the resonance $f_0(1300)$ reveals itself not as a bump or minimum but as a shoulder in the spectrum, had been specially emphasized in [8,13]. No visible structure had been observed in the two-meson spectra from Crystall Barrel reactions $p\bar{p}(at\,rest,liquid\,H_2) \to \pi^0\pi^0\pi^0$, $\pi^0\pi^0$, $\pi^0\eta\eta$, although this state was strongly needed for the combined description of the three-meson Dalitz-plots and the two-pion production reactions [1,3]: the combined fits [5,6,8] provide a strong restriction for the position of this state — it could be not higher than 1350 MeV. The notation $f_0(1370)$ used in the PDG compilation [11] is a tribute to these early (and exaggerated) values ¹.

There is no common belief in the existence of the $f_0(1300)$, and its parameters are supposed to be poorly defined: in the compilation [11] the mass and half-width are quoted as $M \simeq (1200 - 1500)$ MeV and $\Gamma/2 \simeq (75 - 125)$ MeV.

The data with a direct evidence for this state were obtained by the GAMS group [3] where the peak associated with $f_0(1300)$ was clearly seen at large momenta transferred to the target nucleon. (Note that a hint to a smallness of the

¹Note that in [11], at the discussion of the status of $f_0(1370)$, the paper [13] with the most detailed analysis of this resonance was not mentioned.

background at large momentum transfers was given by the $K\bar{K}$ production data [19] where events were collected at $0.2 \le |t| \le 0.5 \text{ GeV}^2$ interval, and a strong bump was seen in the mass region $\sim 1300 \text{ MeV}$).

The GAMS data [3], where a strong enhancement in the spectra was observed in the 1300 MeV mass region, were included into recent K-matrix analyses of the $IJ^{PC}=00^{++}$ -amplitude [8–10]. In [10], the mass $(1300\pm20)-i(120\pm20)$ MeV was found for $f_0(1300)$. It became obvious that exchange by large momenta favours the production of this state, and new measurement of the $\pi^0\pi^0$ spectra at moderately large |t| in the reaction $\pi^-p \to \pi^0\pi^0n$ at $p_{lab}=18~{\rm GeV/c}$ performed by the E852 Collaboration [20] provided an important contribution into verification of parameters of this resonance. The signal from $f_0(1300)$ is clearly seen in the spectra $\pi^0\pi^0$ at $|t|\sim 0.5-1.5~{\rm (GeV/c)^2}$, for, as was said above, the background at such momenta transferred is small.

However, the account for the pion-pair-production data in the K-matrix analysis meets with a poor knowledge of the details of the t-channel exchange mechanism at such momenta. At small momenta, $|t| \lesssim 0.2 \text{ (GeV/c)}^2$, the reggeized pion exchange dominates. At $|t| \sim (0.2-04) \text{ (GeV/c)}^2$, the behaviour of the two-pion production cross section with the growth of |t| changes: the decrease of $d\sigma/dtdM_{\pi\pi}$ becomes less steep. The change of the regime can be due to the onset of different t-channel exchange mechanisms at moderate |t| such as multi-reggeon rescatterings, say, $\pi P, \pi PP$, and so on (P denotes the Pomeron) or to the contribution of the a_1 exchange and related branchings such as a_1P, a_1PP , etc.

In [4], by performing the K-matrix analysis of the GAMS $\pi\pi$ -spectra in the vicinity of the $f_0(980)$, the t-distributions were approximated by the effective pion exchange. It was supposed that at small |t| the reggeized pion exchange dominates, while at increasing |t| the change of regime is accompanied by a change of sign in the amplitude (recall that the πP branching changes the amplitude sign). In the analysis [9] of the $\pi\pi$ spectra in the region of $f_0(980)$ and $f_0(1300)$, a scenario with a large contribution of the reggeized a_1 exchange at |t| > 0.5 (GeV/c)² was realized in the K-matrix fit. The hypothesis that the change of regime in the t-distribution at $M_{\pi\pi} \sim 1000$ MeV is due to the a_1 exchange was also discussed in [21].

To decrease the uncertainties related to a poor knowledge of the t-channel exchange mechanism, the $M_{\pi\pi}$ -distributions averaged over a broad t-intervals $|t_1| \leq |t| \leq |t_2|$ were used in [4] to fit to data:

$$\frac{\langle d\sigma \rangle}{dM_{\pi\pi}} = \int_{t_1}^{t_2} dt \frac{d\sigma}{dt dM_{\pi\pi}} , \qquad (1)$$

for the t-intervals as follows: 0 < |t| < 0.2, 0.3 < |t| < 1.0, 0.35 < |t| < 1.0, 0.4 < |t| < 1.0, 0.45 < |t| < 1.0, 0.5 < |t| < 1.0 (GeV/c)². The averaged distributions, as one may believe, are not sensitive to the details of the t-distribution, as the averaging over a broad momentum-transfer interval makes smoother the particularities of t-distributions. Fitting to the spectra confirmed this statement [9,10]. In the analysis of t-distributions [9], where, together with pion exchange, the a_1 reggeized exchange was included, the parameters of the $f_0(980)$ and $f_0(1300)$ appeared to be weakly sensitive to different entries of the t-channel exchange mechanism, thus giving us a hope that a reliable determination of resonance pole singularities as well as pole residues (associated with partial widths) are possible in the framework of the averaging procedure (1).

Recent measurements of the $M_{\pi\pi}$ spectra in the reaction $\pi^-p \to \pi^0\pi^0 n$ at |t| < 1.5 (GeV/c)² [20] provide us an opportunity to enlighten the t-channel mechanism as well as to study to what extent the averaging of spectra (1) makes the extracted resonance parameters insensitive to the details of t-exchange mechanism. The present paper is devoted to the consideration of these problems.

As in previous studies [4–6,9,10], we analyse the $\pi\pi$ spectra in terms of the K-matrix amplitude. Because of that, in Section 2 we recall the necessary K-matrix technique formulae. Section 3 presents the results of the fit. In Conclusion we summarize our understanding on the t-channel exchange mechanism and recall the properties of the $f_0(980)$ and $f_0(1300)$ resonances found in the K-matrix analysis based on the spectra measured by GAMS group [3] and E852 Collaboration [20].

II. THE K-MATRIX AMPLITUDE

In this Section we present the formulae for the K-matrix analysis of the 00^{++} wave. The given analysis is a continuation of earlier work [8–10]. In the latter paper [10] the 00^{++} wave had been reconstructed on the basis of the following data set:

- (1) GAMS data on the S-wave two-meson production in the reactions $\pi p \to \pi^0 \pi^0 n$, $\eta \eta n$ and $\eta \eta' n$ at small nucleon momenta transferred, $|t| < 0.2 \text{ (GeV/}c)^2 [3,22,23]$;
- (2) GAMS data on the $\pi\pi$ S-wave production in the reaction $\pi p \to \pi^0 \pi^0 n$ at large momenta transferred, $0.30 < |t| < 1.0 \text{ (GeV/}c)^2 [3,22];$

- (3) BNL data on $\pi p^- \to K\bar{K}n$ [24];
- (4) Crystal Barrel data on $p\bar{p}$ (at rest, liquid H_2) $\to \pi^0\pi^0\pi^0$, $\pi^0\pi^0\eta$, $\pi^0\eta\eta$ [12,25].

Now the experimental basis has been much broadened, and additional samples of data are included into current analysis of the 00^{++} wave, as follows:

- (5) Crystal Barrel data on proton-antiproton annihilation in gas: $p\bar{p}$ (at rest, gaseous H_2) $\to \pi^0\pi^0\pi^0$, $\pi^0\pi^0\eta$, $\pi^0\eta\eta$
- (6) Crystal Barrel Data on proton-antiproton annihilation in liquid H_2 : $\pi^+\pi^-\pi^0$, $K^+K^-\pi^0$, $K_SK_S\pi^0$ [26]; (7) Crystal Barrel data on neutron-antiproton annihilation in liquid deuterium $n\bar{p}$ (at rest, liquid D_2) $\to \pi^0\pi^0\pi^-$, $\pi^-\pi^-\pi^+, K_SK^-\pi^0, K_SK_S\pi^-$ [26];
- (8) E852 Collaboration data on the $\pi\pi$ S-wave production in the reaction $\pi^-p \to \pi^0\pi^0n$ for nucleon momentum transfers squared $0 < |t| < 1.5 \,(\text{GeV/c}^2)$ [20].

Below we set out the K-matrix formulae used for the data analysis of the S-wave in the reaction $\pi^- p \to (\pi \pi)_S n$.

A. The K-matrix scattering amplitude for the 00^{++} partial wave

The K-matrix technique is used for the description of the two-meson coupled channels:

$$\hat{A} = \hat{K}(\hat{I} - i\hat{\rho}\hat{K})^{-1},\tag{2}$$

where \hat{K} is $n \times n$ matrix (n is the number of channels under consideration) and \hat{I} is the unity matrix. The phase space matrix is diagonal: $\hat{\rho}_{ab} = \delta_{ab}\rho_a$. The phase space factor ρ_a is responsible for the threshold singularities of the amplitude: to keep the amplitude analytical in the physical region under consideration we use analytical continuation for ρ_a below threshold. For example, the $\eta\eta$ phase space factor $\rho_{\eta\eta} = (1 - 4m_{\eta}^2/s)^{1/2}$ is equal to $i(4m_{\eta}^2/s - 1)^{1/2}$ below $\eta\eta$ threshold (s is the two-meson invariant energy squared). To avoid false singularity in the physical region, we use for the $\eta\eta'$ channel the phase space factor $\rho_{\eta\eta'} = (1 - (m_{\eta} + m_{\eta'})^2/s)^{1/2}$. For the multi-meson phase volume in the isoscalar sector, we use the four-pion phase space defined as either $\rho\rho$ or

 $\sigma\sigma$ phase space, where σ denotes the S-wave $\pi\pi$ amplitude below 1.2 GeV. The result does not depend practically on whether we use $\rho\rho$ or $\sigma\sigma$ state for the description of multi-meson channel: below we provide formulae and the values of the obtained parameters for the $\rho\rho$ case, for which the fitted expressions are less cumbersome.

For the S-wave amplitude in the isoscalar sector, we use our standard parametrization [6,8,10]:

$$K_{ab}^{00}(s) = \left(\sum_{\alpha} \frac{g_a^{(\alpha)} g_b^{(\alpha)}}{M_{\alpha}^2 - s} + f_{ab} \frac{1 \text{ GeV}^2 + s_0}{s + s_0}\right) \frac{s - s_A}{s + s_{A0}} , \qquad (3)$$

with the following notations for meson states: $1 = \pi\pi$, $2 = K\bar{K}$, $3 = \eta\eta$, $4 = \eta\eta'$ and 5 = multi-meson states (four-pion state mainly at $\sqrt{s} < 1.6$ GeV). The $g_a^{(\alpha)}$ is a coupling constant of the bare state α to the meson channel; the parameters f_{ab} and s_0 describe the smooth part of the K-matrix elements ($s_0 > 1.5 \text{ GeV}^2$). We use the factor $(s-s_A)/(s+s_{A0})$ to suppress the effect of the false kinematical singularity at s=0 in the amplitude near the $\pi\pi$ threshold. Parameters s_A and s_{A0} are kept to be of the order of $s_A \sim (0.1-0.5)m_\pi^2$ and $s_{A0} \sim (0.1-0.5)$ GeV² (note that the upper limit of s_{A0} coincides with the position of the ρ -meson left-hand singularity); for these intervals the results do not depend practically on precise values of s_A and s_{A0} .

For the two-meson states, $\pi\pi$, $K\bar{K}$, $\eta\eta$, $\eta\eta'$, the phase space matrix elements are equal to:

$$\rho_a(s) = \sqrt{\frac{s - (m_{1a} + m_{2a})^2}{s}} \qquad , \qquad a = 1, 2, 3, 4 \tag{4}$$

where m_{1a} and m_{2a} are masses of the pseudoscalars. The multimeson phase space factor is defined as

$$\rho_5(s) = \begin{cases} \rho_{51} & \text{at } s < 1 \text{ GeV}^2, \\ \rho_{52} & \text{at } s > 1 \text{ GeV}^2, \end{cases}$$
 (5)

$$\rho_{51} = \rho_0 \int \frac{ds_1}{\pi} \int \frac{ds_2}{\pi} M^2 \Gamma(s_1) \Gamma(s_2) \sqrt{(s+s_1-s_2)^2 - 4ss_1} \times$$

$$\times s^{-1}[(M^2-s_1)^2+M^2\Gamma^2(s_1)]^{-1}[(M^2-s_2)^2+M^2\Gamma^2(s_2)]^{-1},$$

$$\rho_{52} = \left(\sqrt{\frac{s - 16m_\pi^2}{s}}\right)^n .$$

Here s_1 and s_2 are the two-pion energies squared, M is ρ -meson mass and $\Gamma(s)$ is its energy-dependent width, $\Gamma(s) = \gamma \rho_1^3(s)$. The factor ρ_0 provides the continuity of $\rho_5(s)$ at $s = 1 \text{ GeV}^2$. The power parameter n is taken to be 1, 3, 5 for different variants of the fitting; the results are weakly dependent on these values (in our previous analysis [10] the value n = 5 was used).

B. The S-wave $\pi\pi$, $K\bar{K}$, $\eta\eta$ and $\eta\eta'$ production in the high-energy πp collisions

Here we present formulae for the high-energy S-wave production of $\pi\pi$, $K\bar{K}$, $\eta\eta$, $\eta\eta'$ at small and moderate momenta transferred to the nucleon. In [3,20,22–24], the πp collisions were studied at $p_{beam} \sim (15-40)$ GeV/c (or $s_{\pi N} \simeq 2m_N p_{beam} \sim 30-80$ GeV²). At such energies, two pseudoscalar mesons are produced due to the t-channel exchange by reggeized mesons belonging to the π and a_1 trajectories, leading and daughter ones.

The π and a_1 reggeons have different signatures, $\xi_{\pi} = +1$ and $\xi_{a1} = -1$. Accordingly, we write the π and a_1 reggeon propagators as:

$$e^{i\frac{\pi}{2}\alpha_{\pi}(t)} \frac{s_{\pi N}^{\alpha_{\pi}(t)}}{\sin(\frac{\pi}{2}\alpha_{\pi}(t))} \quad , \qquad ie^{-i\frac{\pi}{2}\alpha_{a1}(t)} \frac{s_{\pi N}^{\alpha_{a1}(t)}}{\cos(\frac{\pi}{2}\alpha_{a1}(t))} \quad . \tag{6}$$

Following [27], we use for leading trajectories:

$$\alpha_{\pi(leading)}(t) \simeq -0.015 + 0.72t, \quad \alpha_{a1(leading)}(t) \simeq -0.10 + 0.72t,$$
 (7)

and for daughter ones:

$$\alpha_{\pi(daughter)}(t) \simeq -1.10 + 0.72t, \quad \alpha_{a1(daughter)}(t) \simeq -1.10 + 0.72t.$$
 (8)

Here the slope parameters are in GeV. In the centre-of mass frame, which is the most convenient for the consideration of reggeon exchanges, the incoming particles move along the z-axis with momentum p. In the leading order of the 1/p expansion, the spin factors for π and a_1 trajectories read:

$$\pi - \text{trajectory}: \quad (\vec{\sigma}\vec{q}_{\perp}), \tag{9}$$

$$a_1 - \text{trajectory}: \quad i(\vec{\sigma}\vec{n}_z)$$

where $\vec{n}_z = \vec{p}_{beam}/p_{beam}$ and \vec{q}_{\perp} is the momentum transferred to the nucleon $(t \simeq -q_{\perp}^2)$. The Pauli matrices $\vec{\sigma}$ work in the two-component spinor space for the incoming and outgoing nucleons: $(\varphi_{out}^* \vec{\sigma} \varphi_{in})$ (for more detail see, for example, [28,29]). Consistent removal from the vertices (9) of the terms decreasing with $p \to \infty$ is necessary for a correct inclusion of the daughter trajectories which should obey, similar to the leading ones, the constraints imposed by the t-channel unitarity condition.

In our calculations, we modify conventionally reggeon propagators in (6). We replace:

$$s_{\pi N} \to \frac{s_{\pi N}}{s_{\pi N0}} , \qquad (10)$$

where the normalization parameter $s_{\pi N0}$ is of the order of 4–20 GeV². To eliminate the poles at t < 0 we introduce additional factors into the reggeon propagators, the Gamma-functions, by replacing in (6):

$$\sin\left(\frac{\pi}{2}\alpha_{\pi}(t)\right) \to \sin\left(\frac{\pi}{2}\alpha_{\pi}(t)\right) \Gamma\left(\frac{\alpha_{\pi}(t)}{2} + 1\right) , \tag{11}$$

$$\cos\left(\frac{\pi}{2}\alpha_{a1}(t)\right) \to \cos\left(\frac{\pi}{2}\alpha_{a1}(t)\right) \Gamma\left(\frac{\alpha_{a1}(t)}{2} + \frac{1}{2}\right).$$

The K-matrix amplitude for the transitions $\pi R(t) \to \pi \pi$, $K\bar{K}$, $\eta \eta$, $\eta \eta'$, $\pi \pi \pi \pi$, where R(t) refers to reggeon, reads:

$$\hat{A}_{\pi R} = \hat{K}_{\pi R} (\hat{I} - i\hat{\rho}\hat{K})^{-1},\tag{12}$$

where $\hat{K}_{\pi R}$ is the following vector:

$$K_{\pi R,b}^{00} = \left(\sum_{\alpha} \frac{G_{\pi R}^{(\alpha)}(t)g_b^{(\alpha)}}{M_{\alpha}^2 - s} + F_{\pi R,b}(t) \frac{1 \text{ GeV}^2 + s_{R0}}{s + s_{R0}}\right) \frac{s - s_A}{s + s_{A0}} . \tag{13}$$

Here $G_{\pi R}^{(\alpha)}(t)$ and $F_{\pi R,b}(t)$ are the reggeon t-dependent form factors. The following limits are imposed on the form factors:

$$G_{\pi\pi}^{(\alpha)}(t \to m_{\pi}^2) = g_{\pi\pi}^{(\alpha)}, \qquad F_{\pi\pi,a}(t \to m_{\pi}^2) = f_{\pi\pi,a},$$
 (14)

where $g_{\pi\pi}^{(\alpha)}$ and $f_{\pi\pi,a}$ enter the matrix element (3).

Different parametrizations of the form factor t-dependence were investigated in our analysis. First, the t-dependence of the form factors is introduced in the exponential form (denoted as A-parametrization):

$$G_{\pi R}^{(\alpha)}(t) = g_{\pi R} \exp\left(\beta_R^{(\alpha)}(t - m_{\pi}^2)\right) , \qquad F_{\pi \pi, a}(t) = f_{\pi \pi, a} \exp\left(\gamma_a(t - m_{\pi}^2)\right) .$$
 (15)

Here, for the sake of simplicity, we have used the same slopes, γ_{α} , for non-resonance K-matrix terms in the channels $\eta\eta$, $\eta\eta'$ and $\pi\pi\pi\pi$. Also for the trajectories $a_{1(leading)}$, $\pi_{(daughter)}$, $a_{1(daughter)}$, the non-resonance couplings were set to be zero.

In the second type of parametrization denoted as B, a more complicated t-dependence has been used for the π trajectory: it is assumed to be a two-term exponential form for the form factor:

$$G_{\pi\pi}^{(\alpha)} = g_{\pi\pi} \left[\left((1 - \Lambda) \exp\left(\beta_1^{(\alpha)} (t - m_\pi^2)\right) + \Lambda \exp\left(\beta_2^{(\alpha)} (t - m_\pi^2)\right) \right] . \tag{16}$$

$$G_{\pi\pi}^{(\alpha)} = g_{\pi\pi} \left[\exp\left(\beta_1^{(\alpha)} (t - m_\pi^2)\right) + \Lambda(t - m_\pi^2) \exp\left(\beta_2^{(\alpha)} (t - m_\pi^2)\right) \right] . \tag{17}$$

The parametrization C assumes a weaker decrease with |t| for the second term, that corresponds to the so-called Orear behaviour [30]:

$$G_{\pi\pi}^{(\alpha)} = g_{\pi\pi} \left[(1 - \Lambda) \exp\left(\beta_1^{(\alpha)} (t - m_\pi^2)\right) + \Lambda \exp\left(-\beta_2^{(\alpha)} \sqrt{|t - m_\pi^2|}\right) \right] , \tag{18}$$

$$G_{\pi\pi}^{(\alpha)} = g_{\pi\pi} \left[\exp\left(\beta_1^{(\alpha)} (t - m_{\pi}^2)\right) + \Lambda(t - m_{\pi}^2) \exp\left(-\beta_2^{(\alpha)} \sqrt{|t - m_{\pi}^2|}\right) \right] . \tag{19}$$

The other form-factor terms are treated in the same way as in the parametrization A. As was said above, the change of regime at $|t| > 0.5 \text{ (GeV/c)}^2$ is possible due to multi-Pomeron exchanges, thus leading to the Orear behaviour, see [31] and references therein.

III. RESULTS

In this Section we present the K-matrix analysis results related to the reactions $\pi^- p \to (\pi \pi)_S n$ at $p_{lab} = 38 \text{ GeV/c}$ [3] and $\pi^- p \to (\pi \pi)_S n$ at $p_{lab} = 18 \text{ GeV/c}$ [20].

In the PWA analysis performed by the E852 Collaboration [20] two solutions had been found. We are fitting to the first one which is called in [20] a physical solution because of its characteristics at the low-mass region. However, near 1100 MeV both solutions give close results, thus creating a problem of separating these solutions above 1100 MeV. Therefore, along with fitting to the first solution, we have performed the analysis where in the mass region higher than 1100 MeV the points of the second solution are used. It occured that fitting to this modified second solution has not led to any qualitative change as compared to the first solution but a non-significant re-definition of parameters for the t-dependence of reggeon form factors. It is reason for not presenting parameters for the modified second solution, and we restrict ourselves only by the discussion of the results obtained from fitting to the first E852 solution.

A. The description of the $M_{\pi\pi}$ - and t-distributions in the reaction $\pi p \to (\pi\pi)_S n$ at 0 < |t| < 1.5 (GeV/c)²

A comparison of the spectra obtained at $p_{lab}=38~{\rm GeV/c}$ [3] and $p_{lab}=18~{\rm GeV/c}$ [20] points to a change of the t-dependence behaviour with energy. This is clearly seen in Fig. 1, where the E852 data are plotted in the interval $|t|=0.3-0.4~{\rm (GeV/c)^2}$ vesus the difference of GAMS spectra for the intervals $|t|=0.3-1.0~{\rm (GeV/c)^2}$ and $|t|=0.4-1.0~{\rm (GeV/c)^2}$ (unfortunately the E852 data are presented for other t intervals than those measured by GAMS). A strong difference of spectra is seen for $M_{\pi\pi} \sim 1100-1350~{\rm MeV}$, that reveals a significant contribution of daughter trajectories into formation of $M_{\pi\pi^-}$ and t-distributions.

The description of data with form factors parametrized in the form A is shown in Figs. 2 and 3, and the corresponding t-dependence of the K-matrix coupling constants is presented in Fig. 4 (normalization constant being $s_{\pi N0} = 4 \text{ GeV}^2$). In this solution, the a_1 exchange is responsible for the peak at 1-GeV region, while the peak at 1300 MeV at large |t| is due to the π daughter trajectory. At |t| between 0.1 and 0.4 GeV², the $a_{1(leading)}$ and $\pi_{(daughter)}$ contributions are responsible for a small peak at 1000 MeV region. For this solution the form factors do not cross the abscissas, see Fig. 4; that means the description of spectra is reached in terms of Regge poles, without Regge branchings. The description of GAMS data is quite satisfactory in this approach (see Fig. 3), although certain deviation is observed at small |t| in the mass region below 1000 MeV. The $f_0(1300)$ at large |t| is mainly described by the $\pi_{(daughter)}$ trajectory exchange. For this solution the $a_{1(leading)}$ contribution is rather large at small |t| providing noticeable deviation from the one-term unitarized amplitude.

Futher improvement can be obtained with the form factor parametrizations for the π -trajectory in the form B: figures 5, 6, 7 demonstrate the results for one of the variants of this parametrization. For the variant shown in Figs. 5, 6, 7, which we denote as B1, we omitted the $a_{1(daughter)}$ trajectory. The $a_{1(leading)}$ -exchange is quite large at $|t| \leq 0.4$ GeV². At rather large |t| the $\pi_{(leading)}$ and $\pi_{(daughter)}$ trajectories are responsible for the peak in the 1300 MeV mass region. The $\pi_{(leading)}$ -exchange is also responsible for the peak at 1000 MeV while $a_{1(leading)}$ -exchange becomes here very small. For this solution the pion-exchange form factors for the states $f_0^{bare}(720)$, $f_0^{bare}(1230)$ and $f_0^{bare}(1600)$ cross the abscissas, thus corresponding to the πP branching effective contribution. The coupling of the $f_0^{bare}(1230)$ state grows with |t| due to the increase of relative weight of the $f_0(1300)$ at large |t|. However, the description of the GAMS data within the parametrization B1 at small t-region is not perfect, see Fig. 6. Adding the $a_{1(daughter)}$ trajectory leads to a noticeable improvement of the description.

Adding the $a_{1(daughter)}$ trajectory, we obtained the solution shown in Figs. 8, 9, 10 (parametrization B2); it has no visible problems with the description of either E852 or GAMS data. For the $\pi_{(leading)}$ exchanges, this solution is similar to those found in our previous analyses [9,10] by fitting to GAMS data only: two resonance couplings cross the abscissas at moderate |t|.

We have also fitted to data under the assumption that the change of the t-distribution structure at |t| > 0.4 $(\text{GeV/c})^2$ is due to the onset of the Orear regime, eqs. (18) and (19). For this case (parametrization C) the results are close to those of the B parametrization, so we do not present here the $M_{\pi\pi^-}$ and t-distributions.

B. Resonance pole positions for the $f_0(980)$ and $f_0(1300)$ states

Using the found solutions, we have determined the positions of pole corresponding to the resonances $f_0(980)$ and $f_0(1300)$:

$$(1031 \pm 10) - i(35 \pm 6) \text{ MeV}$$
, $(1315 \pm 20) - i(150 \pm 30) \text{ MeV}$. (20)

The pole for the $f_0(980)$ is under the $\pi\pi$ and $\pi\pi\pi\pi$ cuts, the closest physical region to this pole is located below the $K\bar{K}$ threshold (for more details concerning the determination of sheets, see [10]).

Recall that in the previous K-matrix analysis [10] we obtained for $f_0(1300)$ the mass value $(1300 \pm 20) - i(120 \pm 20)$ MeV, while for the $f_0(980)$ it was $(1015 \pm 15) - i(43 \pm 8)$ MeV. One can see that the magnitudes quoted in [10] and (20) agree reasonably with each other.

By fitting to data on the two-meson spectra at $|t| \sim 0.5 - 1.0$ (GeV/c)², we should definitely recognize that our a priory knowledge about the t-channel exchange mechanism is poor. In the considered t-region, together with the Regge pole terms (π and a_1 exchanges), the Regge branching contributions with additional pomeron-induced interactions (πP , $\pi P P$, or $a_1 P$, $a_1 P P$, etc. t-channel exchanges) are to be significant. The contribution of Regge branchings is enhanced at moderately large |t|, this circumstance was known long ago, see e.g. [31,32]. The presence of a number of terms in the t-channel exchange mechanism at $|t| \gtrsim 0.5$ (GeV/c)² makes the model-independent reconstruction of the t-channel amplitude hardly plausible. Hence a necessity appears to use at moderately small momentum transfers the $M_{\pi\pi}$ -distributions, which are not sensitive to the details of the t-channel mechanism. Let us stress once again

that, in our opinion, the $M_{\pi\pi}$ -distributions averaged over a broad interval of momentum transfers do respond to the problem of finding masses and widths of the resonances.

IV. CONCLUSION

We have performed the fitting to data to determine parameters of the $f_0(980)$ and $f_0(1300)$ observed in the $(\pi\pi)_S$ spectra in the reaction $\pi^-p \to (\pi\pi)_S n$ [3,20] by checking several hypotheses about the |t| exchange mechanism.

Concerning the structure of the |t|-channel exchange mechanism, one can see that the E852 data satisfy well the suggestion about reggeized π -exchange dominating small momentum transfers, $|t| < 0.2 \text{ (GeV/c)}^2$, this very mechanism worked at GAMS energies as well [4]. With the increase of |t|, the change of regime occurs, and the E852 data definitely confirm this. Yet, the details of the change of regime remain unclear: this may happen due the inclusion of the a_1 -exchange, or the branchings πP , $a_1 P$ (P is the Pomeron), or even due to multiple rescatterings (the Orear regime). The E852 data reveal that at $|t| > 0.2 \text{ (GeV/c)}^2$ the daughter trajectories (pion or a_1 -meson) contribute significantly, and the change of the structure of |t|-distributions with energy definitely proves it.

The fitting procedure uses the $M_{\pi\pi}$ spectra which are averaged over certain intervals of |t|. With different inputs for the t-channel exchange mechanism at $|t| \simeq 0.4 \,(\text{GeV/c})^2$, we have observed a stability of the resonance parameters found for $f_0(980)$ and $f_0(1300)$, and they are close to those obtained in previous analysis [10]. So our analysis does not confirm the statement of the paper [33] about a strong dependence of extracted parameters on the details of the t-channel exchange mechanism at $|t| \geq 0.4 \,(\text{GeV/c})^2$.

ACKNOWLEDGEMENT

We are grateful to A.V. Anisovich, D.V. Bugg, L.G. Dakhno and V.A. Nikonov for useful and stimulating discussions. The paper is supported by the RFBR grant No 01-02-17861.

- [1] G. Grayer et al., Nucl. Phys. B75, 189 (1974).
- [2] D. Aston et al., Nucl. Phys. B**296**, 493 (1988).
- [3] Yu.D. Prokoshkin et al., Physics-Doklady **342**, 473 (1995).
- [4] V.V. Anisovich, A.A. Kondashov, Yu.D. Prokoshkin, S.A. Sadovsky, and A.V. Sarantsev, Phys. Lett. B355, 363 (1995).
- [5] V.V.Anisovich and A.V.Sarantsev, Phys. Lett. B 382, 429 (1996).
- V.V. Anisovich, Yu.D. Prokoshkin, and A.V. Sarantsev, Phys. Lett. B 389, 388 (1996).
- [7] A.V. Anisovich and A.V. Sarantsev, Phys.Lett. B 413 137 (1997).
- [8] V.V. Anisovich, UFN **168**, 481 (1998), [Physics-Uspekhi **41**, 419 (1998)].
- [9] V.V. Anisovich, D.V. Bugg and A.V. Sarantsev, Yad. Fiz. 62, 1322 (1999) [Physics of Atomic Nuclei, 62, 1247 (1999)].
- [10] V.V. Anisovich, A.A. Kondashov, Yu.D. Prokoshkin, S.A. Sadovsky, A.V. Sarantsev, Yad. Fiz. 60, 1489 (2000) [Phys. Atom. Nucl. 60, 1410 (2000)].
- [11] D.E. Groom et al. (Particle Data Group), Eur. Phys. J. C15, 1 (2000).
- [12] V.V. Anisovich, D.S. Armstrong, I. Augustin, et al. (Crystal Barrel Collaboration), Phys. Lett. B323, 233 (1994).
- [13] V.V. Anisovich, D.V. Bugg, A.V. Sarantsev, and B.S. Zou. Phys. Rev. D50, 1972 (1995); "How to solve the three-pion annihilation problem", Contribution to the Conference "NN Interaction, Annihilation and Scattering", Moscow, October 1993, published in Yad. Fiz. 57, 1666 (1994) [Phys. Atom. Nucl. 57, 1595 (1994)].
- [14] D.V. Bugg, V.V. Anisovich, A.V. Sarantsev and B.S. Zou, Phys. Rev. **D50**, 4412 (1994).
- [15] I.J.R. Aitchison, Phys. Rev. 133, 1257 (1964);
 - B.N. Valuev, Zh. Exp. Teor. Fiz. 47, 649 (1964) [Sov. Phys. JETP 20, 433 (1965)];
 - V.V. Anisovich, L.G. Dakhno, Phys. Lett. 10, 221 (1964); Nucl. Phys. 76, 665 (1966);
 - A.V. Anisovich, V.V. Anisovich, Phys. Lett. **B345**, 321 (1995).
- [16] C. Amsler et al., Phys. Lett. **B291**, 347 (1992).
- [17] R. Kamenski et al., Phys. Rev. **D50**, 3145 (1994).
- [18] K.L. Au, D. Morgan, M.R. Pennington, Phys. Rev. **D35**, 1633 (1987).
- [19] V.A. Polychronakos et al. Phys. Rev., D19m 1317 (1979),
 - A.D. Martin and E.N.Ozmultu, Nucl. Phys., B158, 520 (1979).
- [20] J. Gunter et al. (E582 Collaboration), hep-ex/0001038.

- [21] N.N. Achasov and G.N. Schestakov, Yad. Fiz. 62, 548 (1999).
- [22] D. Alde et al., Zeit. Phys. C66, 375 (1995);
 A.A. Kondashov et al., in it Proc. 27th Intern. Conf. on High Energy Physics, Glasgow, 1994, p. 1407;
- [23] F. Binon et al., Nuovo Cim. A78, 313 (1983); A80, 363 (1984).
- [24] S.J. Lindenbaum and R.S. Longacre, Phys. Lett. **B274**, 492 (1992);
 A. Etkin et al., Phys. Rev. D **25**, 1786 (1982).
- [25] C. Amsler et al. (Crystal Barrel Collaboration), Phys. Lett. B342, 433 (1995); B355, 425 (1995).
- [26] E. Klempt and A.V. Sarantsev, private communication.
- [27] A.V. Anisovich, V.V. Anisovich, and A.V. Sarantsev, Phys. Rev. D 62:051502 (2000).
- [28] A.B. Kaidalov and B.M. Karnakov, Yad. Fiz. 11, 216 (1970).
- [29] G.D. Alkhazov, V.V. Anisovich and P.E. Volkovitsky, "Diffractive interaction of high energy hadrons with nuclei", Chapter I, "Science", Leningrad, 1991.
- [30] J. Orear, Phys. Lett. 13, 190 (1964).
- [31] V.V. Anisovich and O.A. Khrustalev, Yad. Fiz. 9, 1258 (1969); 12, 1262 (1970).
- [32] A.A. Anselm, I.T. Dyatlov, Yad. Fiz. 6, 591 (1967).
- [33] N.N. Achasov, G.N. Shestakov, hep-ph/0107243 (2001).

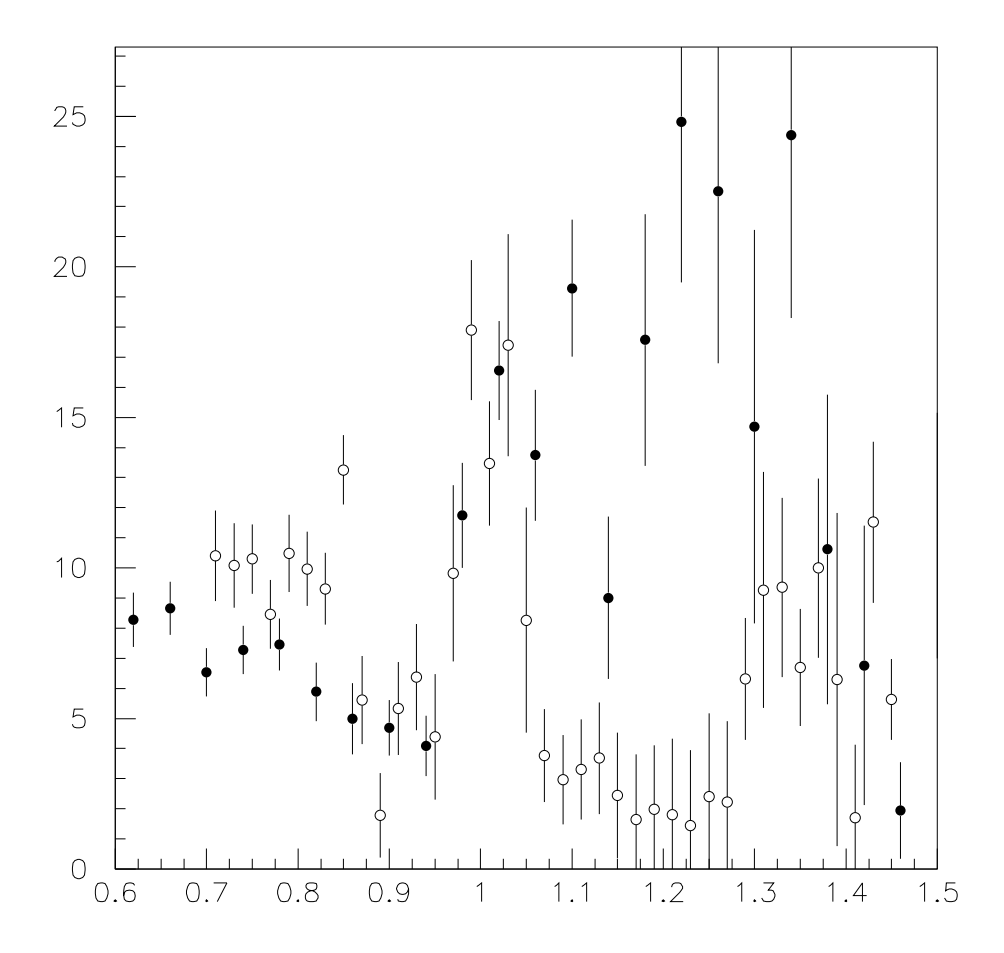


Fig. 1. Comparison of the GAMS and E852 data for the |t|-interval $0.3 \le |t| \le 0.4 \text{ (GeV/c)}^2$. The full circle are E852 data and open circles correspond to the subtraction of two sets of GAMS data, $|t| = 0.3 - 1.0 \text{ (GeV/c)}^2$ and $|t| = 0.4 - 1.0 \text{ (GeV/c)}^2$.

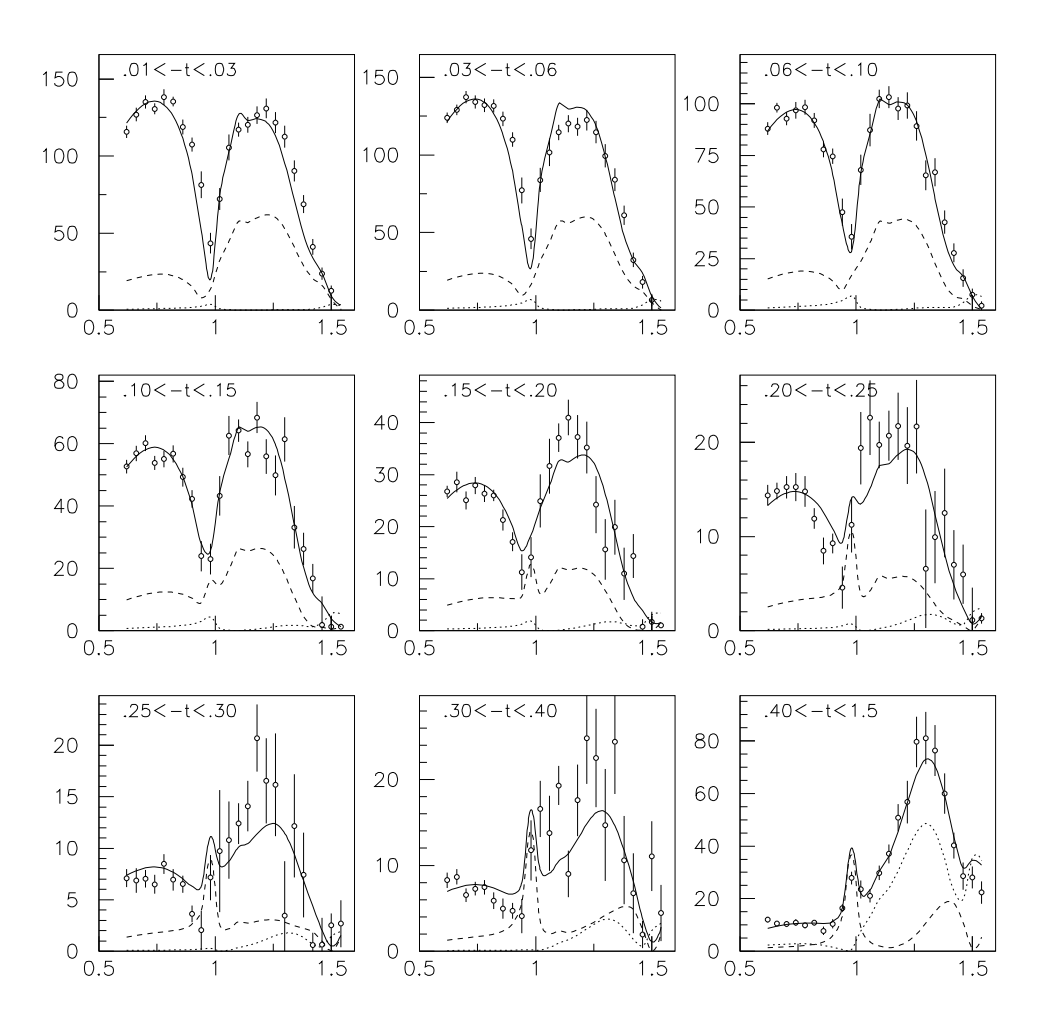


Fig. 2. Description of the E852 data in different t-intervals for solution A. Dashed and dotted curves show the contribution of $a_{1(leading)}$ and $\pi_{(daughter)}$ trajectories, correspondingly.

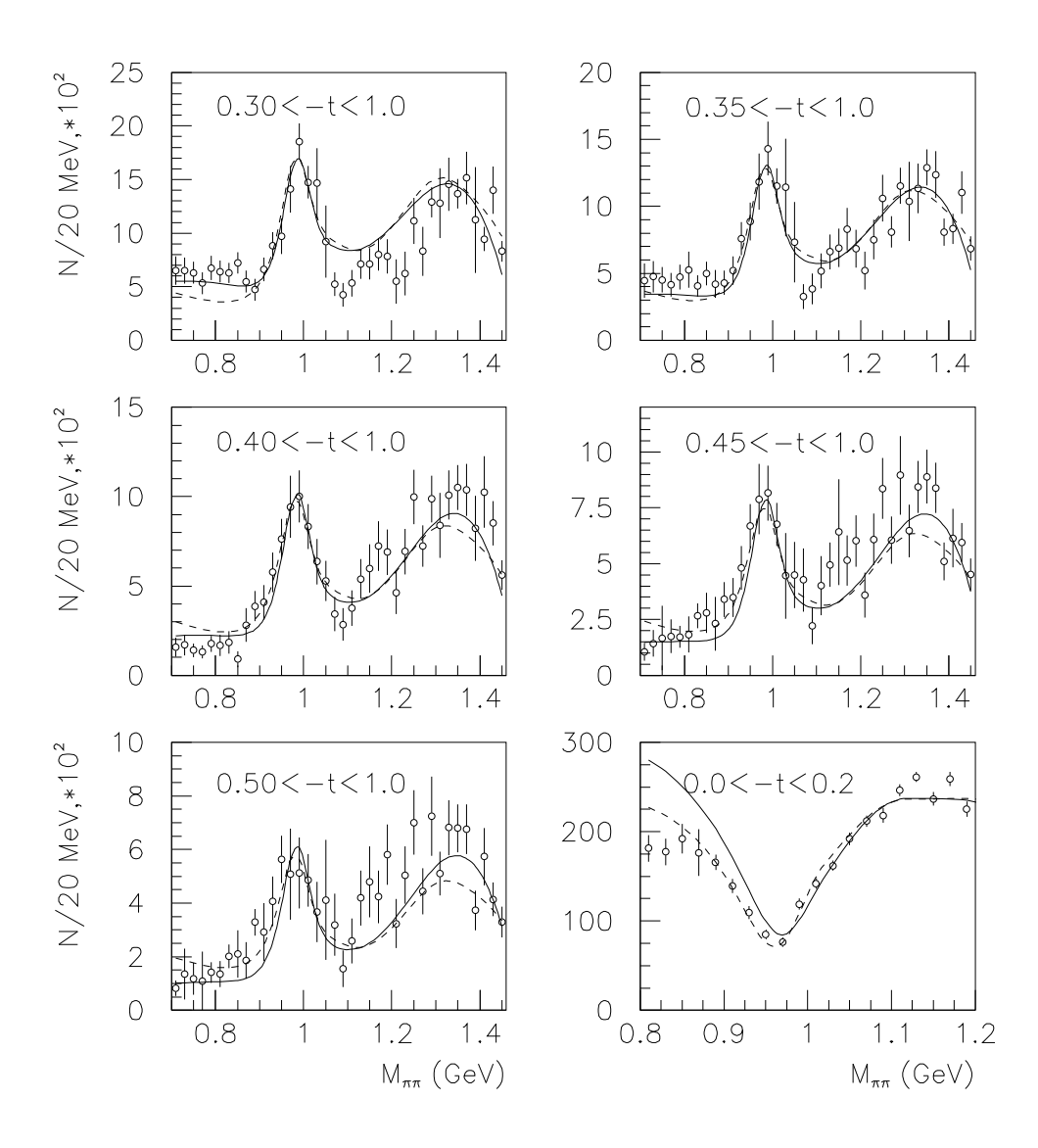


Fig. 3. Description of the GAMS data in different t-intervals for coupling parametrization in the form A. Dashed line shows the solution published previously [10] for the fit of GAMS data alone.

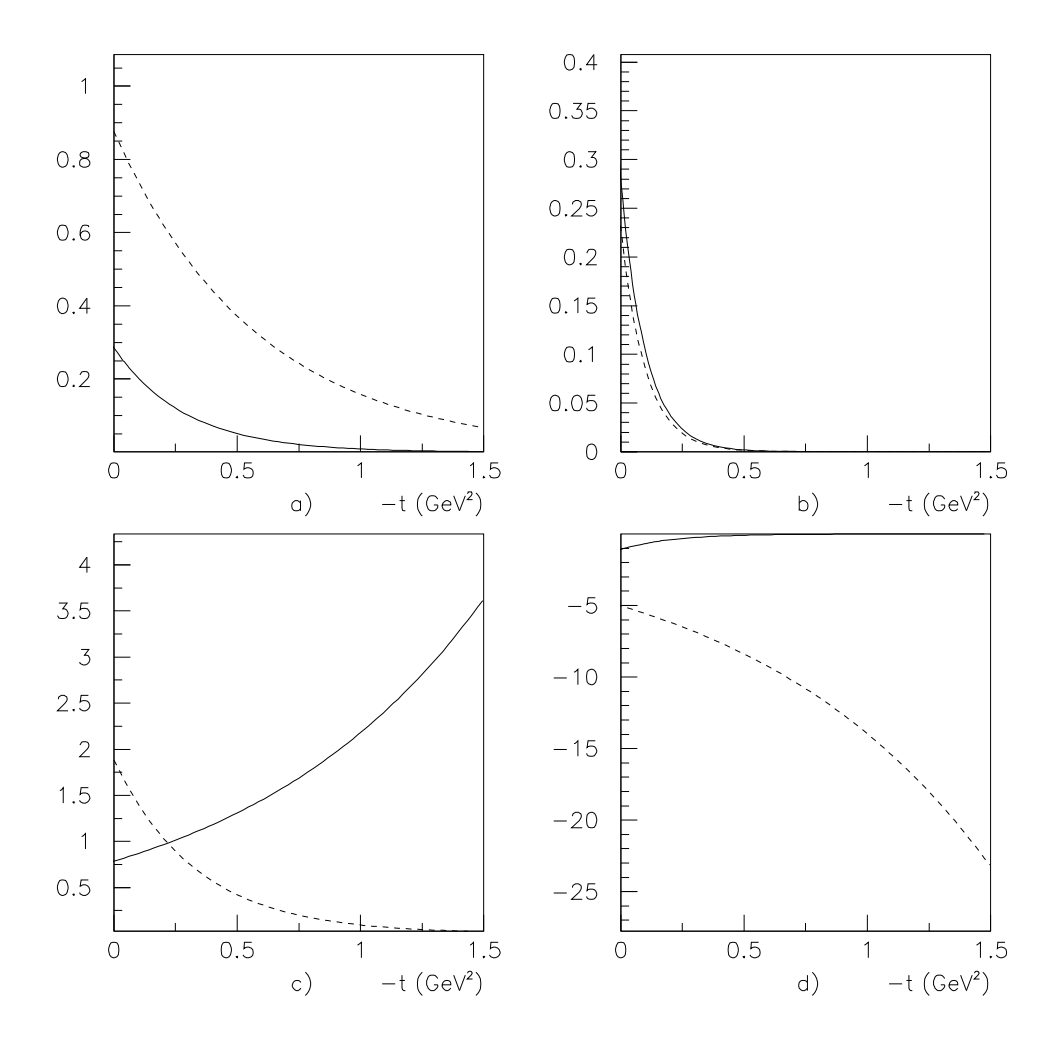


Fig. 4 The t-dependence of the K-matrix couplings for the $\pi_{(leading)}$ exchange in the solution A: a) full curve for $f_0^{bare}(720)$ and dashed one for $f_0^{bare}(1250)$, b) full curve for $f_0^{bare}(1600)$ and dashed curve for $f_0^{bare}(1230)$. c), d) t-dependence of the same vertices for the $a_{1(leading)}$ -trajectory exchange (notations are the same as in Fig. 4a, b).

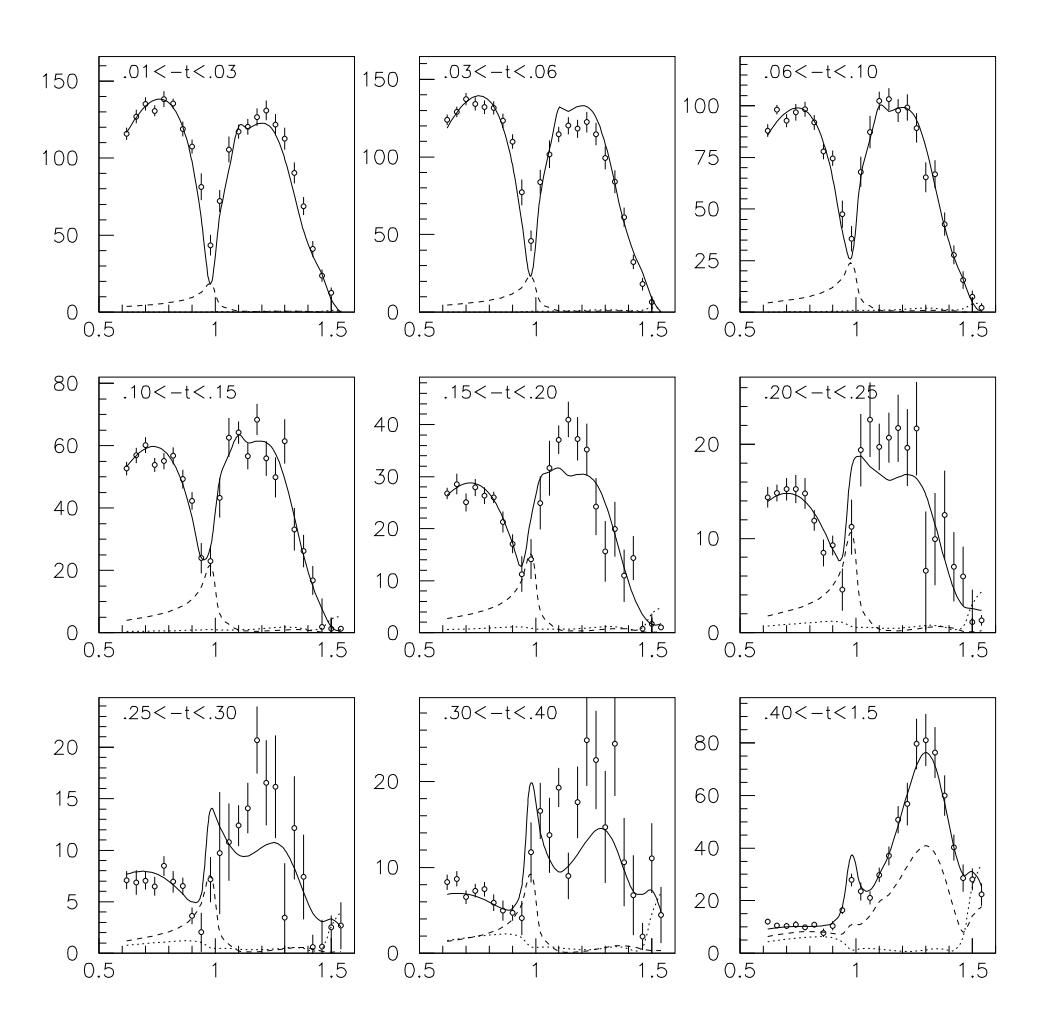


Fig. 5. The same as in Fig. 2 but for the solution B1.

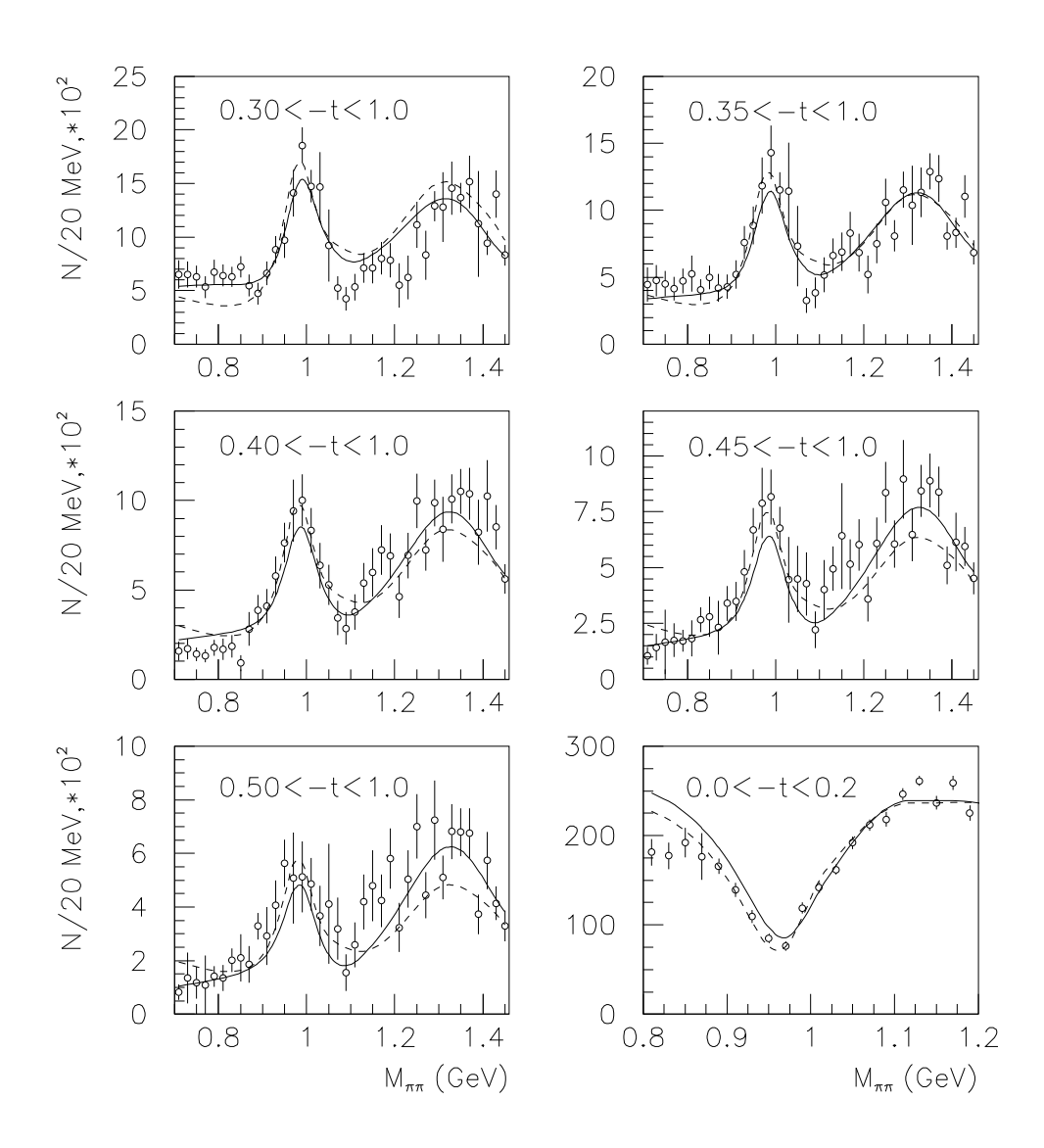


Fig. 6. The same as in Fig. 3 but for the solution B1.

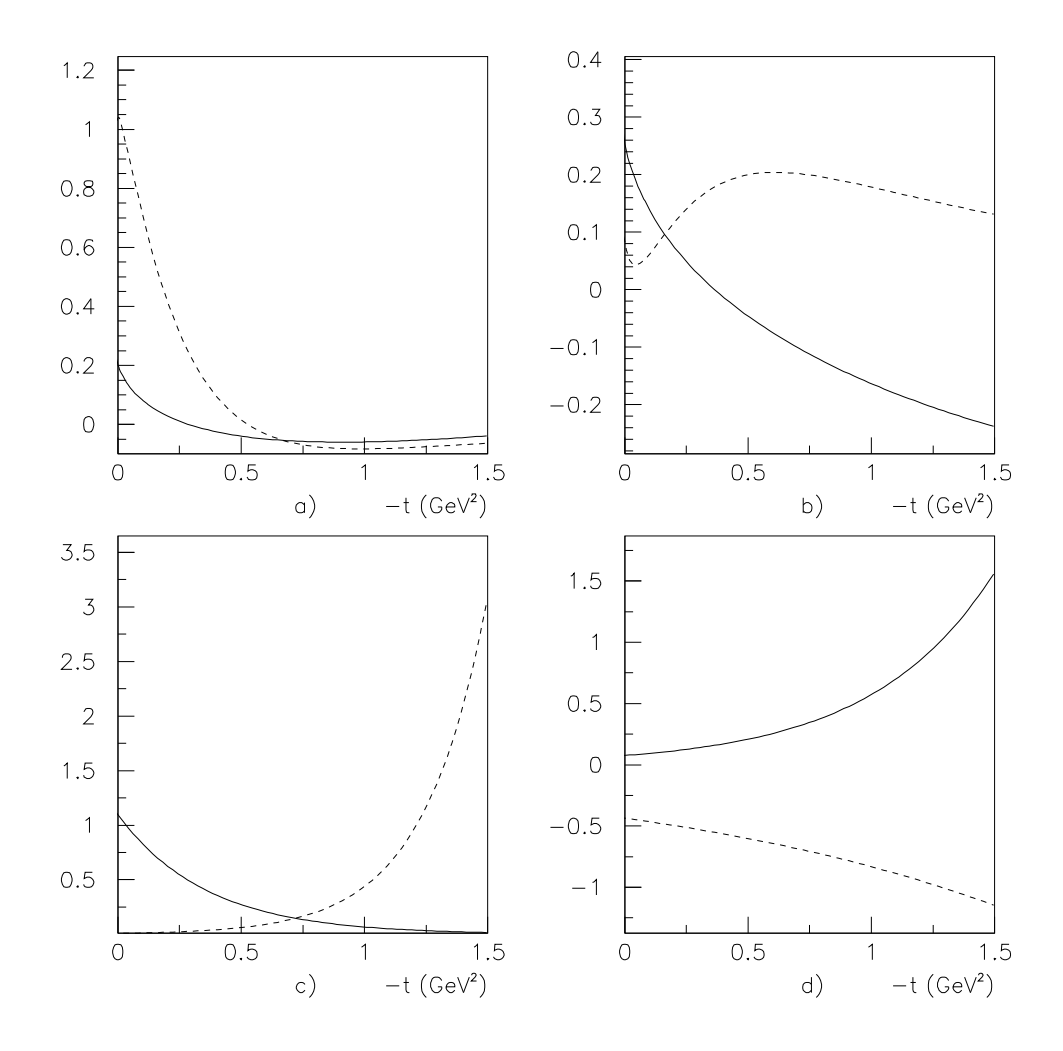


Fig. 7. The same as in Fig. 4 but for the solution B1.

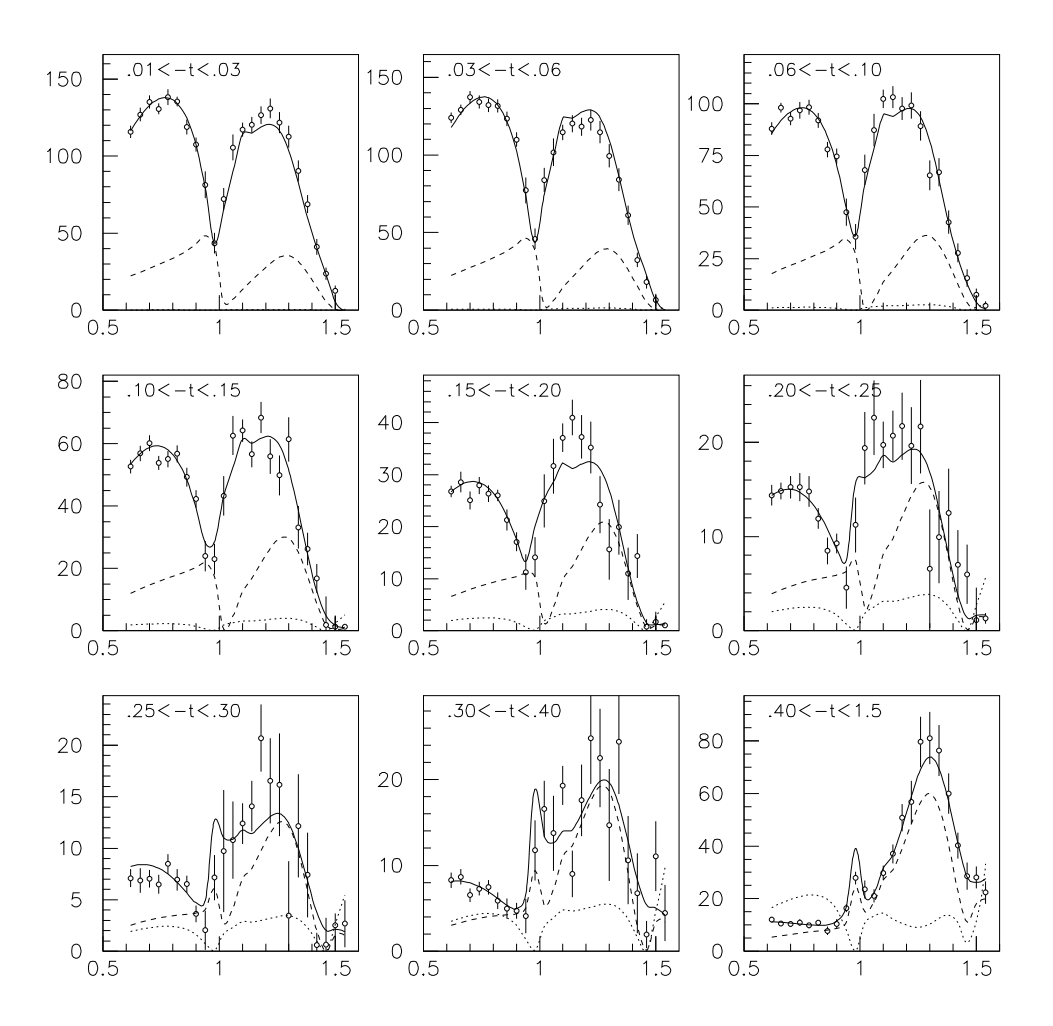


Fig. 8. The same as in Fig. 2 but for the solution B2.

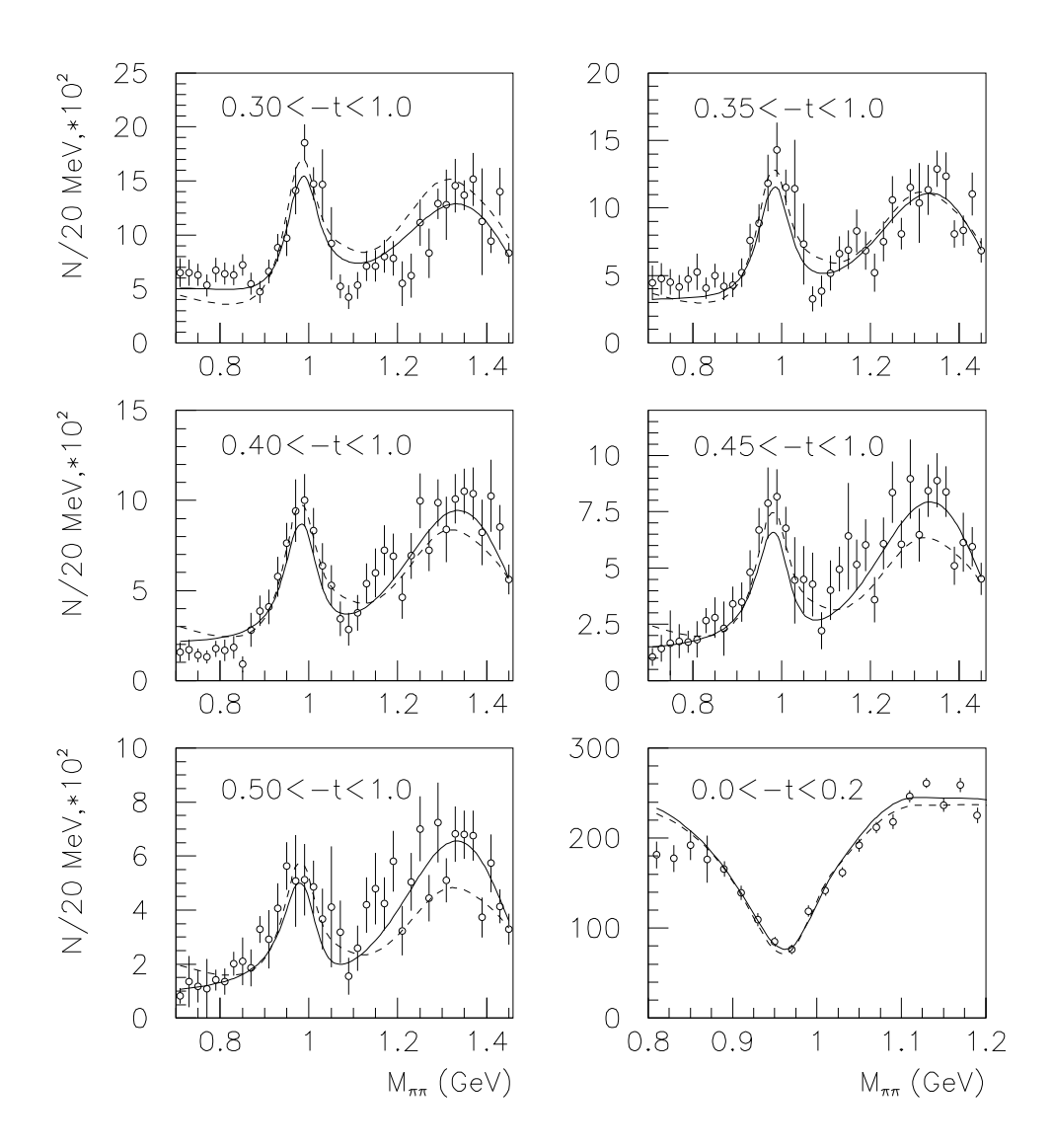


Fig. 9. The same as in Fig. 3 but for the solution B2.

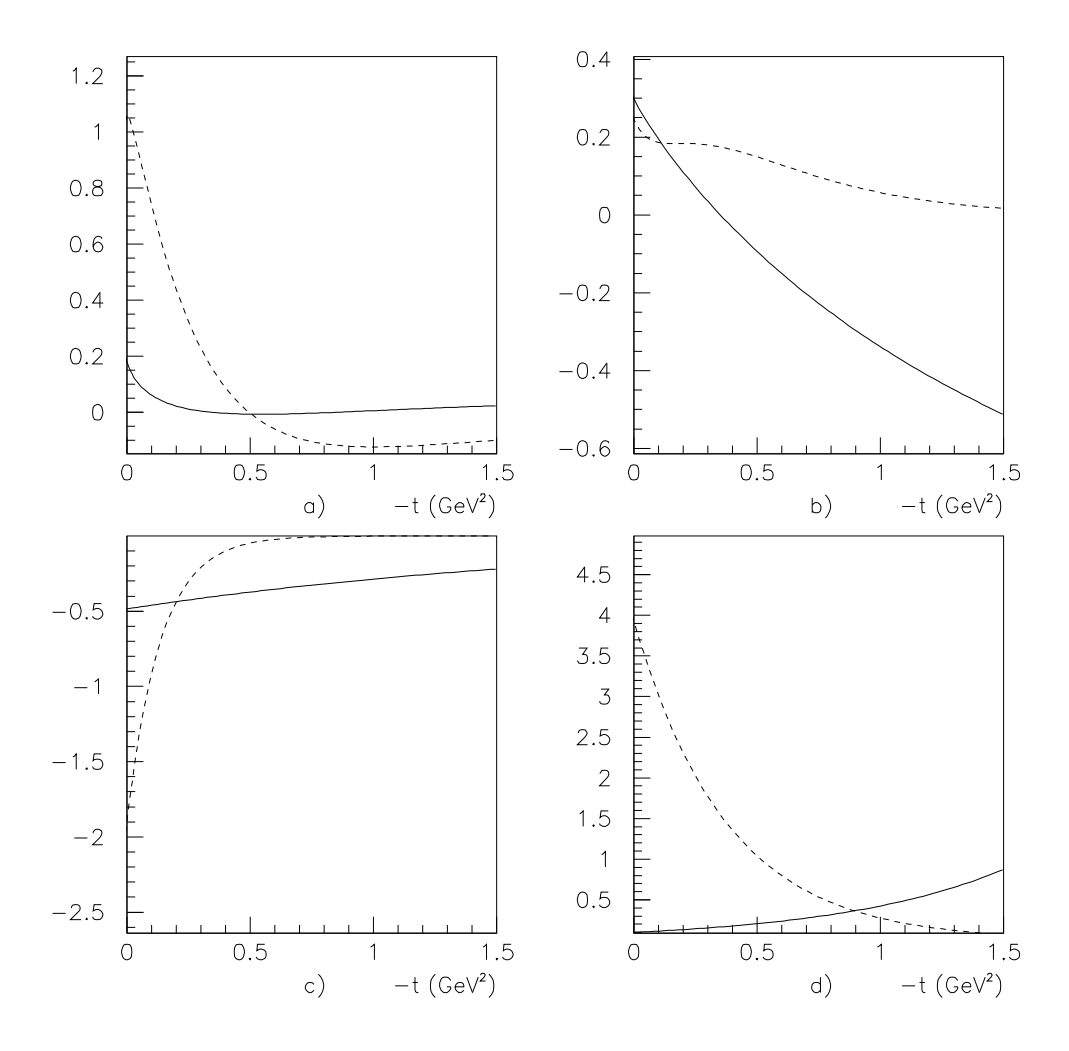


Fig. 10. The same as in Fig. 4 but for the solution B2.